Analytical Methods

ROYAL SOCIETY OF CHEMISTRY

PAPER

View Article Online
View Journal | View Issue

Cite this: *Anal. Methods*, 2025, **17**, 6598

Comparative evaluation of positive and negative LC-MS modes for DOM profiling†

Jiying Pei,[a] Shiguo Chen,[b] Jiayu Zhang,[a] Wenfeng Yu,[a] Weijie Qin[a] and Kefu Yu*[a]

Dissolved organic matter (DOM) in marine environments is critical for nutrient cycling and carbon storage, forming a fundamental part of the ocean's biogeochemical cycles. Traditionally, DOM analysis has utilized negative electrospray ionization (ESI−) mass spectrometry, yet positive electrospray ionization (ESI+) mode has recently gained traction. However, few studies have compared ESI+ and ESI− to understand how these modes impact the overall DOM profiling results. This study investigates DOM profiles from the Sansha Yongle Blue Hole (SYBH)—the world's deepest blue hole—using HPLC-Orbitrap-MS/MS in both ESI+ and ESI− modes. Results show that ESI+ detects a broader range of DOM ions, with a significant correlation in ion counts between the two modes across different depths. ESI+ is more effective for detecting nitrogen-rich compounds (CHN, CHON, CHONS), while ESI− is better for sulfur-rich compounds (CHOS), especially in anoxic layers. Both modes identify similar levels of carbohydrates, carboxyl-rich alicyclic molecules (CRAM), and unsaturated aliphatic compounds (UA), but ESI+ detects more highly unsaturated compounds (HU), peptides, and polyphenols. Correlations in ion counts for carbohydrates, CRAM, and UA across depths indicate consistency between modes, while differences for HU, peptides, and polyphenols suggest lower ionization efficiency in ESI−. Both modes distinguish oxic, chemocline, and anoxic layers, but molecular parameters like double bond equivalents (DBE), modified aromaticity index (AImod), and H/C ratios correlate between modes, while O/C ratios do not. These discrepancies suggest that using only one ionization mode may bias DOM interpretation. Future studies should employ multi-mode ionization to enhance DOM profiling and understanding across marine environments.

Received 24th April 2025
Accepted 24th July 2025

DOI: 10.1039/d5ay00679a

rsc.li/methods

1. Introduction

Dissolved organic matter (DOM) is a vital component of the marine biogeochemical cycle, serving as a reservoir of organic carbon and playing a key role in nutrient cycling and energy transfer within marine ecosystems.[1] It is integral to the oceanic food web, mediating the exchange of elements between inorganic reservoirs and the marine biosphere.[2] Additionally, DOM significantly influences microbial interactions, shaping the dynamics of microbial communities and broader ecological processes.[3] Therefore, a comprehensive understanding of DOM is essential for unraveling the complexities of oceanic processes and their connections to the global carbon cycle.

However, characterizing the composition and molecular properties of DOM presents considerable challenges due to its high complexity and heterogeneity.[4] Recent advancements in analytical techniques have facilitated more in-depth exploration of DOM's chemical complexity. Among these techniques, Fourier-transform ion cyclotron resonance mass spectrometry (FT-ICR-MS)[5] and liquid chromatography-tandem mass spectrometry (LC-MS/MS)[6] stand out for their high sensitivity, resolution, and ability to analyze complex mixtures. FT-ICR-MS is particularly valuable for its accurate mass measurements, allowing for unambiguous molecular formula assignments and providing detailed insights into the molecular diversity of DOM.[7] Despite these advantages, elucidating the molecular structure of DOM remains challenging, especially regarding isomers, which limits the ability to determine its origins and cycling pathways in the environment. In contrast, LC-MS/MS offers significant advantages for structural analysis. It enables both level 1 and level 2 structural identification through molecular annotation, thereby enhancing the understanding of DOM's composition. When combined with bioinformatics platforms like GNPS (Global Natural Products Social Molecular Networking), LC-MS/MS expands the scope of DOM structure analysis, facilitating more comprehensive profiling.[8] The incorporation of liquid chromatography (LC) as a pre-separation step further improves analysis by reducing sample complexity and minimizing ion suppression.[9] This is essential for detecting low-abundance compounds and separating isomers while yielding valuable retention time data for more

[a]*Guangxi Laboratory on the Study of Coral Reefs in the South China Sea, Coral Reef Research Center of China, School of Marine Sciences, Guangxi University, Nanning 530004, China. E-mail: kefuyu@scsio.ac.cn*

[b]*School of Resources, Environment and Materials, Guangxi University, Nanning 530004, China*

† Electronic supplementary information (ESI) available. See DOI: https://doi.org/10.1039/d5ay00679a

accurate qualitative and quantitative analyses of DOM.[10] These advanced capabilities are critical for comparing compounds across samples, allowing for deeper insights into the molecular variability of DOM. By leveraging high-resolution LC-MS/MS, researchers can generate comprehensive molecular inventories from complex environmental datasets. This is vital for addressing key questions about the geochemistry of DOM.

In DOM studies, selecting the appropriate ionization mode is critical, as it significantly impacts the types and range of detectable compounds. Traditionally, the negative electrospray ionization (ESI−) mode has been preferred for targeting compounds with acidic functional groups, such as organic acids and phosphates, due to its high ionization efficiency for these species.[11] However, advancements in mass spectrometry have highlighted the increasing importance of the positive electrospray ionization (ESI+) mode. ESI+ enhances ionization efficiency for nitrogen-containing compounds and achieves higher match rates in spectral database searches.[8] For instance, ESI+ has demonstrated strong capabilities in detecting nitrogen-rich xenobiotics, including pharmaceuticals and personal care products, in marine environments.[12] In this content, ESI+ has demonstrated superior performance in compound annotation, offering broader coverage of DOM chemical space compared to ESI−. Despite the distinct advantages of both ionization modes, substantial differences in molecular formula assignments are frequently observed. Recently, several studies have focused on comparing ESI+ and ESI− modes for DOM characterization.[13–16] For example, a study on DOM in Antarctic snow revealed only 1–11% formula overlap between the two modes.[13] Similarly, a study of seawater and freshwater from New Zealand demonstrated that 30% of molecular formulas were shared between the two sample types in ESI−, while over 90% overlapped in ESI+, suggesting that ESI+ captures a broader set of molecular features common across aquatic environments.[14] This study further revealed significant discrepancies in key bulk parameters, such as double bond equivalents (DBE), the element ratios (H/C and O/C), between ionization modes. These findings underscore that each ionization mode reveals distinct aspects of DOM composition, highlighting the importance of careful mode selection to capture comprehensive molecular diversity.[15,16]

However, most existing studies comparing ESI+ and ESI− have primarily focused on general metrics, including the total number of assigned molecular formulas, formula overlap, elemental compositions, and heteroatom distributions. Comparative evaluations at a finer scale—specifically across molecular categories such as carbohydrates, carboxyl-rich alicyclic molecules (CRAM), unsaturated aliphatic compounds (UA), highly unsaturated compounds (HU), peptides, and polyphenols—remain limited. Furthermore, these investigations have largely been confined to standard reference materials,[15] surface waters,[16] or specific matrices like snow,[13] freshwater,[14] or lignin degradation products.[17] There is a notable lack of studies considering how dynamic environmental gradients, especially redox stratification, influence DOM ionization behavior across different modes.

To address this gap, the present study conducts a systematic comparison of ESI+ and ESI− for DOM analysis in the Sansha Yongle Blue Hole (SYBH)—the world's deepest marine blue hole. The SYBH presents a naturally occurring, vertically stratified water column with distinct oxic, chemocline, and anoxic layers,[18] offering an ideal setting to examine how hydrogeochemical gradients influence DOM composition and ionization behavior. By performing a depth-resolved comparison of DOM detected in both ionization modes, this study aims to evaluate the degree of consistency between ESI+ and ESI− in capturing molecular diversity, chemical space coverage, and compositional features. The outcomes will provide critical guidance for future DOM studies in complex marine environments, informing optimal ionization mode selection for comprehensive molecular characterization.

2. Materials and methods

2.1. Sample collection

SYBH is the world's deepest oceanic blue hole, reaching a depth of 300 meters and characterized by its unique vertical structure.[19] The steep walls enclose the central shaft, descending to approximately 50 meters below sea level. Below this depth, the cave's passage angle shifts from nearly vertical (90°) to a steeper slope exceeding 120°, reaching down to 150 meters. Beyond this point, the passage angle gradually returns to 90° as it narrows. This distinct topography limits water exchange between the surface and deeper layers, resulting in significant variations in physical and chemical properties at different depths. Based on oxygen content, the SYBH can be divided into three layers: the oxic layer (<50 m), the chemocline (50–150 m), and the anoxic layer (150–300 m).

In October 2019, 28 seawater samples were collected from SYBH (111.768°E, 16.525°N) (Fig. S1a and 1b†) at various depths, encompassing the oxic layer (0 m, 10 m, 20 m), the chemocline (50 m, 80 m, 85 m, 90 m, 95 m, 100 m, 110 m, 120 m, 150 m), and the anoxic layer (200 m, 250 m) (Fig. S1c†). Each depth was sampled in duplicate. Sampling techniques differed based on depth: a conductivity-temperature-depth (CTD) system with a 12-bottle rosette sampler (General Oceanics, USA) was employed for the oxic layer and chemocline. However, the complex terrain of SYBH limited the winch to a maximum depth of 190 m. To collect samples from the deeper anoxic layer, a remotely operated vehicle (ROV) equipped with GO-Flo bottles (General Oceanics, USA) was used. Environmental parameters, including temperature, salinity, DO, pH, turbidity, and chlorophyll-a (Chl-a), were measured *in situ* across the 0 to 300 m depth range using the CTD system. All seawater samples were filtered on-site using a 0.45 μm pore size membrane filter (Acropak, Pall) and stored at −20 °C for subsequent DOM analysis in the laboratory. The experimental workflow is outlined in Fig. S2.†

2.2. Solid phase extraction

The solid phase extraction (SPE) method followed the protocol developed by Dittmar *et al.*[20] Filtered seawater samples (1.2 L)

were acidified to a pH of 2 using hydrochloric acid (HCl) and concentrated with Agilent Bond Elut PPL cartridges (200 mg, 3 mL). Before loading the samples, the cartridges were conditioned with 8 mL of methanol, followed by 8 mL of acidified Milli-Q water (pH = 2). The seawater was then passed through the cartridges at a flow rate of 4 mL min^{-1}, followed by a rinse with 10 mL of acidified Milli-Q water. After drying the cartridges with nitrogen gas, the DOM was eluted using 8 mL of methanol. The eluent was concentrated to a final volume of 0.5 mL under nitrogen gas and reconstituted with an equal volume (0.5 mL) of Milli-Q water. The final extract was stored at −20 °C until analysis by LC-MS/MS.

2.3. LC-MS/MS data acquisition and pre-processing

The seawater extracts were analyzed using a Thermo Q-Exactive mass spectrometer coupled with a Dionex UltiMate 3000 HPLC system. Chromatographic separation was achieved using an ACQUITY CSH C18 column (2.1 × 100 mm; 1.7 μm particle size; Waters, MA, USA) at a flow rate of 200 μL min^{-1} and a temperature of 30 °C. The mobile phase consisted of H_2O with 0.1% formic acid (mobile phase A) and methanol with 0.1% formic acid (mobile phase B). The gradient profile was as follows: from 0 to 3 minutes, 5% B; from 3 to 20 minutes, a linear increase from 5% to 95% B. The system was held at 95% B for 5 minutes, then returned to 5% B over 1 minute, followed by a 4-minute equilibration before the next injection. A 2 μL injection volume was used for each sample.

Mass spectrometry data were collected using data-dependent acquisition (DDA) in both ESI+ and ESI−. The ESI source parameters were optimized as follows: sheath gas flow, 35 L min^{-1}; auxiliary gas flow, 15 L min^{-1}; auxiliary gas temperature, 250 °C. The spray voltage was set to 3.5 kV for ESI+ and 3.0 kV for ESI−. The inlet capillary temperature was maintained at 350 °C, with an S-lens RF level of 50 V applied to enhance ion transmission. The full mass spectra were scanned from *m*/*z* 100 to 1000, achieving a resolution of 35 000 at *m*/*z* 200 (R*m*/*z* 200). A maximum ion injection time of 100 ms was set, with automated gain control (AGC) configured at 3.0×10^6. In MS/MS mode, the top 10 most intense ions were selected for fragmentation. The MS/MS scans achieved a resolution of 17 500 at *m*/*z* 200 (R*m*/*z* 200), with a maximum ion injection time of 50 ms and AGC set to 1.0×10^5. The precursor selection window for MS/MS was set at *m*/*z* 1.5, with normalized collision energy gradually increasing from 15% to 30%.

Chromatographic peaks, including MS1 features and MS/MS spectra, were extracted from mass spectrometry raw data using MZmine software (version 3.4.27), an open-source tool.[21] The LC-MS/MS raw data are accessible through the Mass Spectrometry Interactive Virtual Environment (**http://massive.ucsd.edu/**) under accession number MSV000080562. Feature extraction employed an exact mass detector with signal thresholds of 70 000 for full MS spectra and 10 000 for MS/MS spectra. The Automated Data Analysis Pipeline (ADAP) chromatogram building used a minimum height of 70 000 and an *m*/*z* tolerance of 0.001 (or 5 ppm). Chromatograms were deconvoluted using the local minimum algorithm, with a peak duration range between 0.07 and 1.20 minutes and a minimum absolute height of 70 000. Isotopic peaks were grouped with an *m*/*z* tolerance of 0.003 Da (or 12 ppm) and a retention time tolerance of 0.05 minutes. Peak alignment was conducted using the Join Aligner Module, applying an *m*/*z* tolerance of 0.02 Da and a retention time tolerance of 0.02 minutes. The final peak list underwent gap filling, utilizing an intensity tolerance of 5%, an *m*/*z* tolerance of 0.001 Da (or 5 ppm), and a retention time tolerance of 0.15 minutes.

2.4. Molecular formula assignment (SIRIUS, ZODIAC) and DOM analysis

The tandem mass spectrometry data exported from MZmine software were annotated using the SIRIUS computational tool. *De novo* molecular formulas were determined using the SIRIUS module, which involved accurate mass calculation, comparison of experimental and predicted isotopic patterns, and analysis of fragmentation trees of the fragment ions.[22] To enhance the accuracy of molecular formula predictions, the ZODIAC module was applied to analyze joint fragments and losses across the fragmentation trees of various compounds in the dataset.[23] The SIRIUS parameters were configured as follows: elements were restricted to carbon (C), hydrogen (H), oxygen (O), nitrogen (N), sulfur (S) and phosphorus (P). A maximum of 10 molecular formula candidates was retained, with the computed maximum precursor ion *m*/*z* set to 600. The instrument type was specified as Orbitrap, and the maximum allowed *m*/*z* deviation was set to 5 ppm. All adducts were considered (auto-charge), and a ZODIAC threshold filter of 0.98 was applied. DOM classification was performed based on the following criteria:[24] carbohydrates, 1.6 < H/C < 2.0, 0.7 < O/C < 1.0, and $N = 0$; CRAM, 0.3 < DBE/C < 0.68, 0.2 < DBE/H < 0.95, and 0.77 < DBE/O < 1.75; UA, 1.5 ≤ H/C < 2, O/C < 0.9, and $N = 0$; HU, AI_{mod} < 0.5, H/C < 1.5, and O/C < 0.9; peptides, 1.5 < H/C < 2.0, O/C ≤ 0.9, and $N > 0$; polyphenols, 0.5 < AI_{mod} < 0.66. The bulk parameters of DOM,[7] including DBE, modified aromaticity index (AI_{mod}), H/C, and O/C, were calculated using the magnitude-weighted average of normalized peak intensities. The normalized intensity of each formula was determined by dividing the peak intensity of each formula by the total intensity of all formulas within each sample.

2.5. Quality control

To ensure the reliability and accuracy of LC-MS/MS analysis for seawater samples, a rigorous quality control protocol was implemented. First, a blank control test was performed to identify any potential contamination during the sample preparation process. In this test, 1.2 L of ultrapure water was subjected to the same extraction procedure as the seawater samples. The signal intensities obtained from the blank control were then subtracted from the corresponding seawater sample intensities to account for background interference. In addition, quality control (QC) samples were prepared by combining 50 mL of seawater from different depths of the SYBH. These pooled samples were processed using SPE, applying the same procedure used for seawater samples. QC samples were

analyzed at regular intervals, specifically after every six seawater samples, to monitor instrument performance and detect any drift or inconsistencies. The relative standard deviation (RSD) range for the remaining 9 characteristic peaks, excluding the 9th peak, is 1.8–7.3% across the five quality control samples (Fig. S3†), indicating acceptable reproducibility within the quality control framework. For data processing, chromatographic peaks exhibiting a standard deviation greater than 30% in the QC samples were excluded to ensure reliability. Prior to instrumental analysis, three consecutive blank injections were made to assess the stability of the instrument and identify any potential background contamination.

2.6. Statistical analysis

Statistical analyses were conducted using multiple software platforms. Principal Component Analysis (PCA) and Orthogonal Partial Least Squares Discriminant Analysis (OPLS-DA) were performed with SIMCA software (version 14.1, Umetrics, Umea, Sweden). Principal Coordinates Analysis (PCoA) was conducted using R packages (version 4.2.2). Statistical significance was assessed with SPSS software (version 23, IBM Corporation, New York, USA). For normally distributed data, Pearson correlation coefficients were calculated to evaluate inter-group correlations, while Spearman correlation coefficients were used for non-normally distributed data. Venn diagrams displaying overlapping compounds across different groups was generated with Venny 2.1, available online at **https://bioinfogp.cnb.csic.es/tools/venny/**. Other statistical analyses were conducted using Origin software (version 2021, OriginLab Corporation, Massachusetts, USA) for tasks not explicitly described.

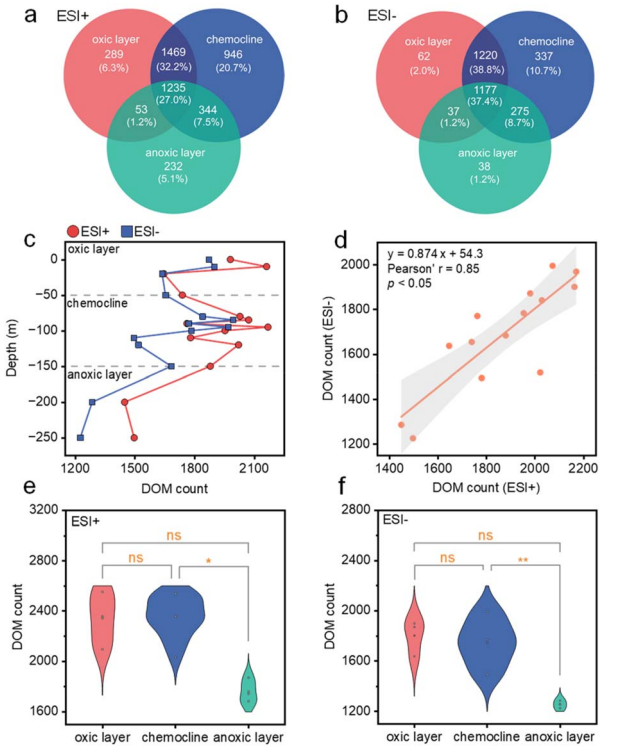

Fig. 1 Venn diagrams showing the distribution of DOM within the oxic layer, chemocline, and anoxic layer under (a) ESI+ and (b) ESI− modes. (c) Variation in DOM counts, and (d) linear correlation analysis of DOM counts, across different depths of the SYBH under ESI+ and ESI− modes. Violin plots displaying DOM counts within the oxic layer, chemocline, and anoxic layer under (e) ESI+ and (f) ESI− modes (* indicates $p < 0.05$, ** indicates $p < 0.01$).

3. Result and discussion

3.1. Comparison of ion features for DOM analysis in ESI+ and ESI− in SYBH

Analysis of DOM in the SYBH using ESI+ and ESI− mass spectrometry revealed distinct ion features across these two modes. The ESI+ mode detected a total of 4568 ions, surpassing the 3146 ions detected in the ESI− mode (Fig. 1a and b). This broader DOM mass spectrum coverage in the ESI+ can be attributed to two main factors. First, acidification with hydrochloric acid increased proton availability, enhancing protonation of organic molecules and thus improving ionization efficiency for ESI+ detection.[25] Second, to enhance the ionization efficiency in the ESI+ mode, low concentrations of acidic reagents are often added to the mobile phase. This not only facilitates protonation reactions but also promotes the formation of various cation adducts.[8] In both ionization modes, most ions were detected in at least two water layers (oxic layer, chemocline, and anoxic layer). In the ESI+, 27.0% of ions were shared across all three layers, while an additional 32.2%, 1.2%, and 7.5% were detected in at least two layers. In contrast, in the ESI−, 37.4% of ions were common across all three layers, with 38.8%, 1.2%, and 8.7% observed in at least two layers. This pattern suggests that the ESI+ has a lower proportion of ions detected across multiple layers (67.9% = 27.0% + 32.2% + 1.2% + 7.5%) than the ESI− (86.1% = 37.4% + 38.8% + 1.2% + 8.7%), resulting in a higher proportion of layer-specific ions in ESI+. For instance, in the oxic layer, 6.3% of ions were unique to the ESI+, compared to only 2.0% in the ESI−. Similarly, in the chemocline, 20.7% of ions were unique to ESI+ *versus* 10.7% in ESI−, and in the anoxic layer, 5.1% were unique to ESI+ compared to 1.2% in ESI−. The more diverse and layer-specific ions observed in ESI+ likely reflects its broader DOM coverage[12] and greater sensitivity to certain molecular classes unique to specific layers, which are less efficiently detected in ESI−.

The distribution of DOM counts across different depths in the SYBH was analyzed in both ESI+ and ESI− to evaluate consistency between the two techniques. As shown in Fig. 1c and d, both modes exhibit a similar trend in DOM counts across depths ($p < 0.05$), suggesting comparable data quality and consistency across ionization methods. This consistency between modes strengthens the reliability of the results. The average DOM counts at the three layers showed that the oxic layer and the chemocline had comparable DOM levels in both ionization modes (Fig. 1e and f). However, both layers exhibited significantly higher DOM counts compared to the anoxic layer. The reduced DOM counts in the anoxic layer can be attributed to two main factors: microbial degradation of DOM and limited water mixing between layers. In the surface layer,

phytoplankton and other organisms produce substantial organic material. As these organisms die, their remains settle through the water column,[26] where microbial activity induces oxidative decomposition, progressively reducing DOM levels with increasing depth.[27] However, limited vertical water mixing prevents the replenishment of DOM in the anoxic layer from the oxygen-rich surface layers. This restricted mixing, coupled with microbial degradation, contributes to the significantly lower DOM counts observed in the anoxic zone.

3.2. Elemental composition of DOM in ESI+ and ESI− in SYBH

DOM can be classified into six categories based on elemental composition: CH, CHO, CHN, CHON, CHOS, and CHONS.[28] Analysis of DOM composition in SYBH across ESI+ and ESI− reveals distinct ionization patterns. Nitrogen-containing compounds (CHN, CHON and CHONS) are more prevalent in ESI+, accounting for 36.9% of the detected compounds (2.0% for CHN, 32.4% for CHON and 2.5% for CHONS), compared to only 10.2% in ESI− (0.1% for CHN, 9.0% for CHON and 1.1% for CHONS) (Fig. 2a). Conversely, CHO and CHOS compounds are more frequently detected in ESI−, with 85.7% of CHO and 4.0% of CHOS detected, compared to 59.1% of CHO and 1.2% of CHOS in ESI+ (Fig. 2a). The absolute detection counts of these six types of DOM in each mode were shown in Fig. 2b. Specifically, CHN compounds (71), CHON compounds (1152) and CHONS compounds (88) are more abundantly detected in ESI+ than in ESI−, where only 3 CHN, 198 CHON and 25 CHONS compounds are observed. In contrast, CHOS compounds are detected more frequently in ESI− (88) than in ESI+ (44). For CH and CHO classes, CHO compounds show higher detection counts in ESI+ (2104 in ESI+ *vs.* 1892 in ESI−), while CH compounds are rare in both modes (99 in ESI+ *vs.* 1 in ESI−). These observations suggest that different ionization modes preferentially ionize specific types of compounds. Nitrogen-containing compounds, such as those with CHN, CHON and CHONS compositions, are more readily protonated in ESI+ due to the higher basicity of nitrogen atoms, which facilitates protonation.[29] In contrast, sulfur-containing compounds, such as those with $-SO_3H$, $-SO_2$, and $-SH$ are more likely to form negative ions in ESI−.[30] This is attributed to the electron-

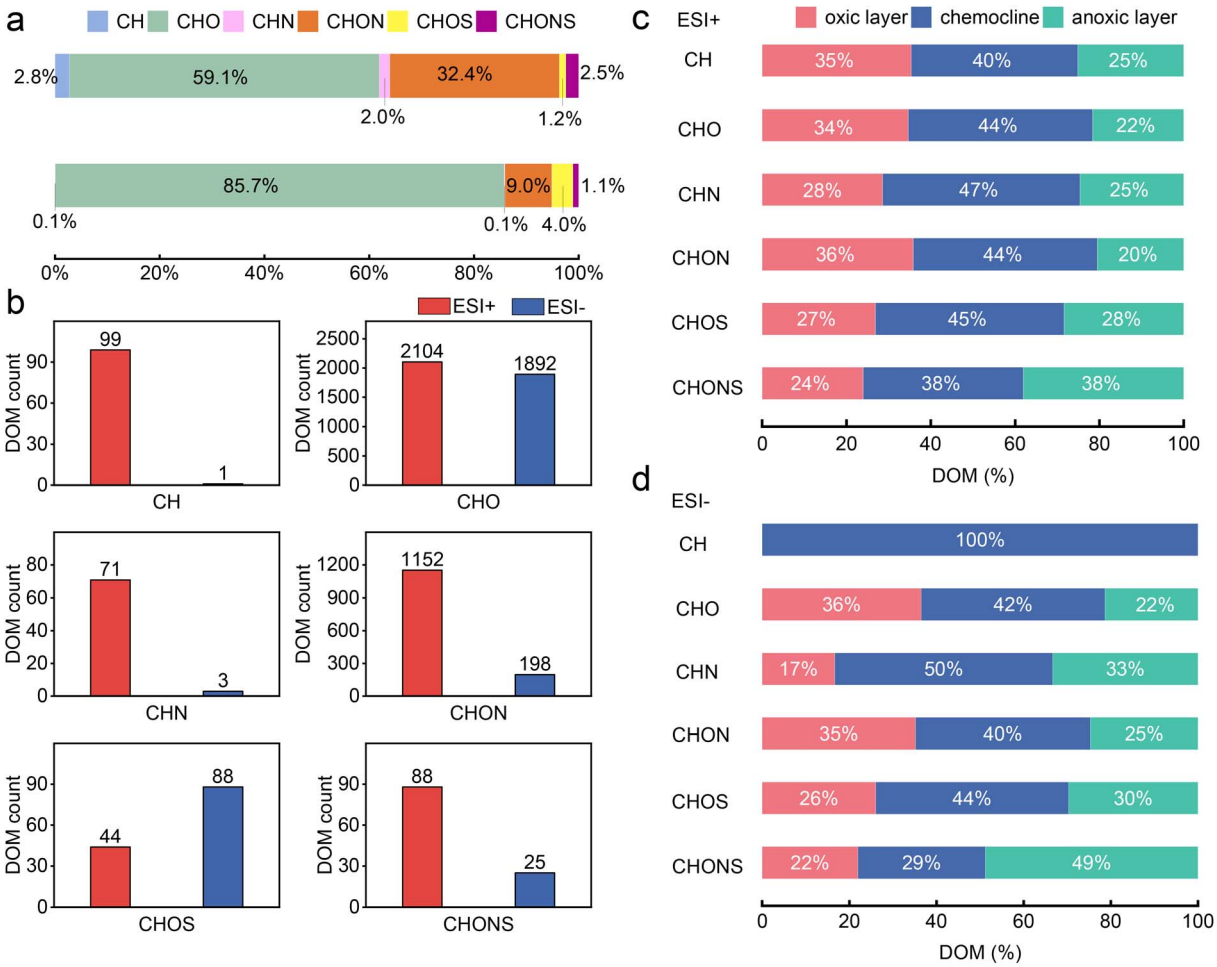

Fig. 2 (a) Molecular elemental composition of DOM in the SYBH under ESI+ and ESI− modes. (b) Count of DOM with elemental composition of CH, CHO, CHN, CHON, CHOS and CHONS under ESI+ and ESI− modes. Distribution of DOM with different elemental compositions across the oxic layer, chemocline, and anoxic layer of the SYBH under (c) ESI+, and (d) ESI− modes.

withdrawing nature of sulfur, which stabilizes negative charges on adjacent atoms and promotes deprotonation.[31] For compounds with a CHO elemental composition, their complex structural diversity leads to some being more readily detected in ESI+, while others are more efficiently ionized in ESI−. Lastly, CH-only compounds are infrequently detected in either ionization mode due to the lack of polar or ionizable functional groups. The slightly higher detection rate in ESI+ may result from alternative ionization mechanisms, such as adduct formation with NH_4^+ or Na^+,[32] or from the lower chemical background noise typically associated with ESI+.

The detection frequencies of six DOM groups (CH, CHO, CHN, CHON, CHOS, and CHONS) across different water layers were analyzed under both ESI+ and ESI− modes (Fig. 2c and d). Across both ionization modes, the chemocline of SYBH consistently showed the highest relative proportions for CH, CHO, CHN, CHON compounds. Conversely, sulfur-containing compounds (CHOS and CHONS) show their highest proportions in the chemocline or anoxic layer under both ionization modes. The elevated levels of CH, CHO, CHN and CHON compounds in the chemocline reflect their overall greater abundance in this layer. As discussed above, this enrichment is probably driven by intense biological activity at the oxic–anoxic interface, including photosynthesis and diverse microbial metabolic processes, which contribute to the generation and transformation of organic metabolites.[33] In contrast, the higher levels of CHOS and CHONS in the chemocline and anoxic layer suggest specific enrichment mechanisms favoring the accumulation of sulfur-containing DOM in oxygen-deprived conditions.[34] These mechanisms likely involve both microbial and abiotic processes. Under anoxic conditions, sulfur-reducing bacteria play a significant role in sulfur transformation, generating sulfur-containing DOM as metabolic byproducts.[35] For example, Patin *et al.* observed an abundance of reduced sulfur compounds produced by sulfur-reducing microorganisms in the oxygen-depleted zones of Amberjack Hole in the Gulf of Mexico.[36] Additionally, abiotic processes further contribute to sulfur DOM accumulation under anoxic conditions.[37] Gomez-Saez *et al.* demonstrated that abiotic reactions between reduced sulfur species and DOM are important contributors to the buildup of sulfur-rich DOM during anoxic events.[38]

It is important to note that compound-specific detection frequencies can be influenced by ionization efficiency. This efficiency may, in turn, be modulated by matrix effects such as salinity and pH gradients with depth.[39] However, these factors are unlikely to significantly affect the vertical distribution patterns observed in this study. Pre-analytical acidification to pH ∼ 2, followed by SPE and LC, substantially attenuates matrix-induced ion suppression, particularly those arising from ionic strength and salt composition.[40] Moreover, the vertical salinity gradient in SYBH is relatively narrow, with values ranging from 33.5‰ to 34.6‰, representing only a 3.3% relative difference (Fig. S4†), thereby further limiting the extent of matrix-driven variability in ionization efficiency across depths.

3.3. Classification of DOM in ESI+ and ESI− in SYBH

DOM in seawater consists of a complex blend of organic compounds. They are generally categorized into six primary types based on their elemental composition and structural features: carbohydrates, CRAM, HU, UA, peptides, and polyphenols.[41,42] Each category exhibits unique chemical characteristics. Carbohydrates are highly oxygenated compounds

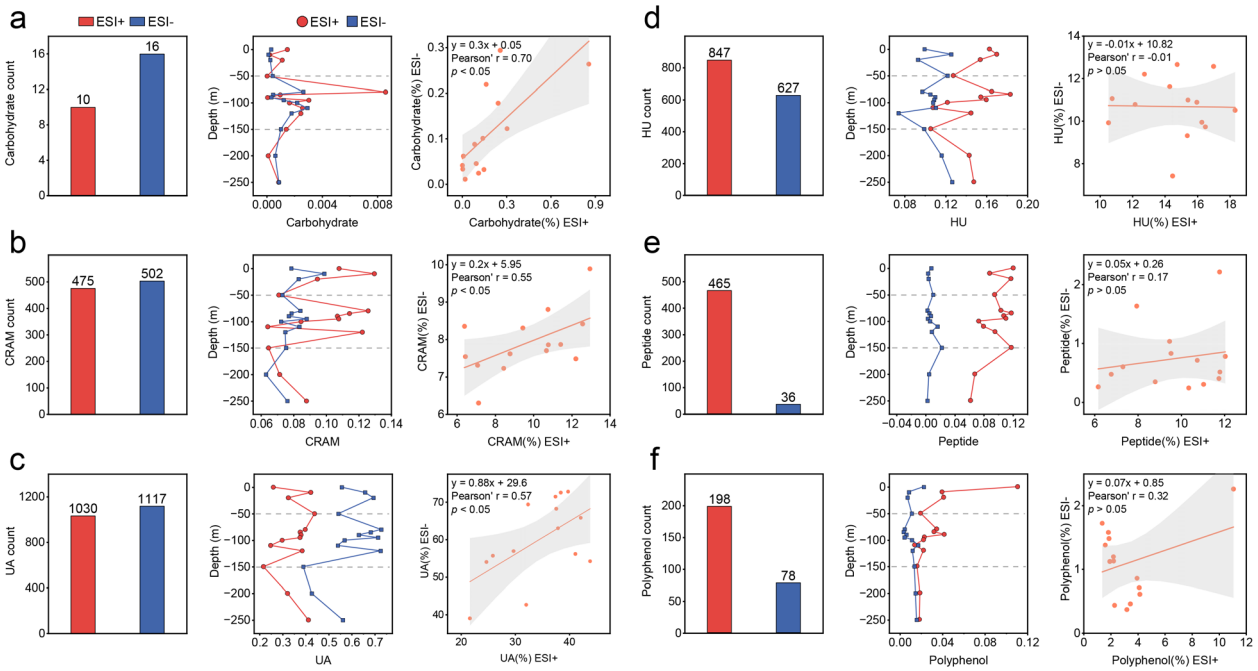

Fig. 3 The count of (a) carbohydrates, (b) CRAM, (c) UA, (d) HU, (e) peptide, and (f) polyphenol in the SYBH under ESI+ and ESI− modes, with variations in abundance at different depths and linear correlation analysis.

devoid of nitrogen atoms and are primarily composed of simple and complex sugars. These compounds typically ionize in ESI+ as $[M + alkali]^+$ and in ESI− as $[M - H]^-$.[43,44] However, carbohydrates have low ionization efficiency in both modes. In DOM samples from SYBH, only 10 carbohydrate ions were detected in ESI+ and 16 in ESI− (Fig. 3a). CRAM, characterized by numerous carboxyl groups, easily lose protons in ESI− due to their acidic nature. They can also gain protons in ESI+ because of the high electronegativity of oxygen atoms. As a result, CRAM showed a balanced detection frequency between the two modes, with 475 ions in ESI+ and 502 ions in ESI− (Fig. 3b). This balance aligns with findings from studies near New Zealand's South Island, where similar counts of CRAM were detected in both ionization modes.[14] UA and HU are both unsaturated compounds, which displayed comparable ion counts in ESI+ and ESI−. For UA, 1030 ions were detected in ESI+ and 1117 ions in ESI− (Fig. 3c). For HU, 847 ions were detected in ESI+ compared to 627 in ESI− (Fig. 3d). Peptides exhibited much higher ionization efficiency in ESI+. This is attributed to their high nitrogen content, particularly amine groups, which readily accept protons. As a result, 465 peptide ions were detected in ESI+, compared to only 36 ions in ESI− (Fig. 3e). Polyphenols also ionized more efficiently in ESI+. This is because their hydroxyl groups are conjugated to aromatic rings, and the electron-rich benzene rings act as electron donors, enhancing the protonation of the hydroxyl oxygen. Consequently, 198 polyphenol ions were detected in ESI+, compared to 78 ions in ESI− (Fig. 3f).

Correlation analysis between ESI+ and ESI− for the six types of DOM in the SYBH revealed distinct distribution patterns across depths. For carbohydrates, CRAM, and UA, their content trends with depth were consistent between the two ionization modes ($p < 0.05$) (Fig. 3a–c). However, no correlation was observed between ESI+ and ESI− for HU, peptides, and polyphenols ($p > 0.05$) (Fig. 3d–f). The consistent trends for the former group are likely due to their balanced detection frequencies across both ionization modes. In contrast, the lack of correlation for the latter group arises from their preferential ionization in ESI+, making ESI− detections unreliable. These findings highlight the importance of considering ionization mode biases when interpreting data, as relying solely on one mode for compounds that predominantly ionize in the other may lead to distorted conclusions about their environmental roles and interactions.

ESI+ data reveal that average concentrations of CRAM, UA, peptides, and polyphenols are lower in the anoxic layer than in the oxic layer. For CRAM and UA, similar vertical patterns were also captured in ESI− mode, consistent with their strong cross-mode correlation. These compounds likely have important ecological functions in stratified aquatic systems. Specifically, CRAM and UA, which are characterized by their chemical recalcitrance, may serve as important contributors to carbon retention in the anoxic zone.[24] Peptides, especially small or cyclic dipeptides, are increasingly recognized for their involvement in microbial signalling.[45] This is supported by our integrated metabolomics and metagenomics data, which show elevated levels of the dipeptide Glu–Phe in the anoxic layer alongside a higher abundance of anaerobic bacteria.[46] Moreover, polyphenols, with their redox activity and microbial reactivity,[47,48] likely influence microbial interactions and nutrient cycling, particularly in the oxic surface waters. Collectively, these results highlight the significant biogeochemical roles of these compound groups in stratified aquatic environments.

3.4. Bulk parameters and molecular profiling for DOM analysis in ESI+ and ESI− in SYBH

In the analysis of DOM, bulk molecular parameters such as DBE, H/C, AI_{mod}, and O/C are critical for evaluating its complexity, reactivity, and environmental significance.[49,50] These parameters offer insight into DOM's molecular structure, particularly regarding unsaturation, aromaticity, and oxidation. The results

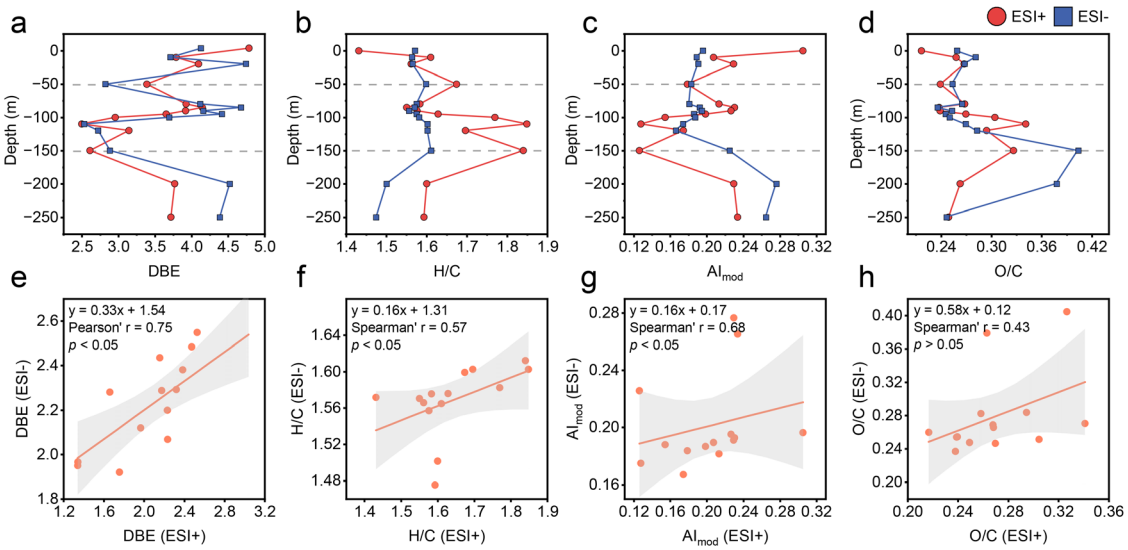

Fig. 4 (a–d) Variation in DBE, H/C, AI_{mod}, and O/C across different depths of the SYBH under ESI+ and ESI− modes. (e–h) Linear correlation analysis of these parameters across different depths of the SYBH between ESI+ and ESI− modes.

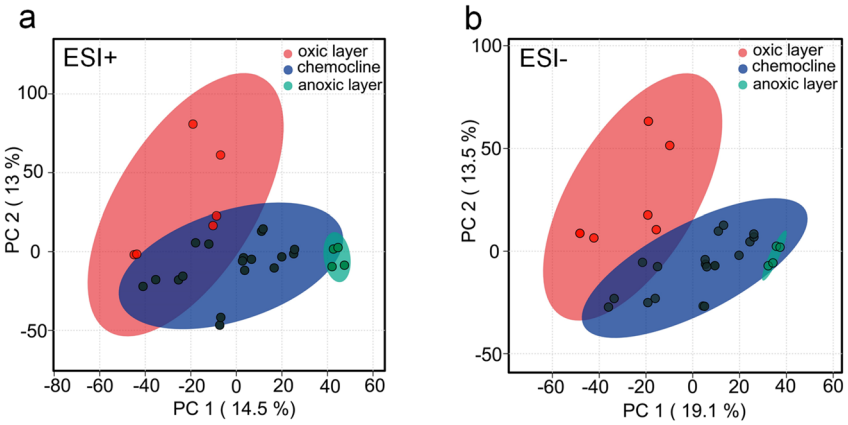

Fig. 5 PCA plots illustrating the differentiation of seawater samples from the oxic layer, chemocline, and anoxic layer of the SYBH under (a) ESI+, and (b) ESI− modes.

showed consistent correlations for DBE, H/C, and AI_{mod} between ESI+ and ESI− modes (Fig. 4a–c, and Fig. 4e–g). This consistency likely arises from the interdependence of these parameters, as they all reflect molecular unsaturation: higher DBE values typically coincide with lower H/C and higher AI_{mod} values, as shown in Fig. S5.† However, the O/C does not display the same consistency across two modes (Fig. 4d and h). It suggests that specific DOM molecular characteristics, such as O/C, may require mode-specific analysis for accurate detection and interpretation.

To explore the compositional differences of DOM across various depths in the SYBH, PCA (Fig. 5), PCoA (Fig. S6†) and OPLS (Fig. S7†) analyses were conducted. The results revealed distinct compositional variations among the oxic, chemocline, and anoxic layers in both ESI+ and ESI− modes. Despite the inherent selectivity of each ionization mode for specific DOM components, the broad molecular coverage provided by both modes enabled effective differentiation of DOM composition across these environmental layers. The vertical stratification of DOM in the SYBH appears to be influenced by the unique environmental conditions at each depth. In the oxic layer, high light availability and elevated oxygen concentrations sustain a diverse community of photosynthetic organisms, such as algae and cyanobacteria, which actively produce DOM.[51] The DOM in this layer is typically fresh, labile, and undergoes rapid biological turnover, resulting in a dynamic pool of readily cycled organic compounds. The chemocline, characterized by steep gradients in oxygen, salinity, temperature, chlorophyll concentration, turbidity, and pH (Fig. S4†), creates a transitional zone where aerobic and anaerobic microbial communities coexist.[52] This zone facilitates diverse metabolic processes, leading to the production of a more complex and heterogeneous DOM pool in the anoxic layer, the absence of oxygen creates a habitat for anaerobic microbes that utilize alternative electron acceptors for metabolism.[53] This results in a distinct DOM composition compared to the oxic layer and chemocline.

4. Conclusions

This study provides a comprehensive comparison of ESI+ and ESI− modes in HPLC-Orbitrap-MS/MS for profiling DOM in the SYBH, highlighting how ionization mode selection influences the detection and interpretation of DOM characteristics. ESI+ captured a broader range of DOM ions than ESI−, although a significant correlation was observed between ion counts detected by both modes across different layers. Elemental composition analysis revealed that nitrogen-rich compounds (CHN, CHON and CHONS) were more abundant in ESI+, while sulfur-rich compounds (CHOS) were preferentially detected in ESI−, particularly in the anoxic layers of the SYBH. Further classification of compounds showed similar detection frequencies for CRAM, UA, and HU across the two ionization modes, while peptides and polyphenols were detected more frequently in ESI+, and carbohydrates consistently showed low detection counts in both modes. Correlation analysis indicated that carbohydrates, CRAM, and UA exhibited significant consistency between ESI+ and ESI− across layers, whereas HU, peptides, and polyphenols showed no correlation. Among bulk molecular parameters, DBE, AI_{mod}, and H/C exhibited consistent correlations between ESI+ and ESI−, while O/C did not, suggesting that specific DOM molecular characteristics may require mode-specific analyses for accurate detection. Despite these discrepancies, both ionization modes effectively differentiated DOM composition across the oxic, chemocline, and anoxic layers of the SYBH. These findings emphasize the importance of using the appropriate ionization mode in DOM analysis. While some parameters yielded consistent results across both modes, others showed significant discrepancies, potentially leading to biased interpretations if only one mode is used. To ensure a more accurate and comprehensive molecular profiling of DOM, we recommend employing multi-mode ionization strategies in future research, enabling a more nuanced analysis of DOM across diverse environmental conditions.

Data availability

Data will be made available on request.

Author contributions

Jiying Pei: writing – review and editing, project administration, funding acquisition, methodology, conceptualization. Shiguo

Chen: writing – original draft, visualization, investigation, formal analysis, software. Kefu Yu: project administration, funding acquisition, resources. Jiayu Zhang: investigation. Wenfeng Yu: supervision. Weijie Qin: software.

Conflicts of interest

There are no conflicts to declare.

Acknowledgements

This work was supported by Guangxi Science and Technology Program (No. AD25069075), Guangxi Natural Science Foundation (No. 2023GXNSFAA026488) and National Natural Science Foundation of China (No. 22264003 and 42090041).

References

1 C. S. Hopkinson and J. J. Vallino, Efficient export of carbon to the deep ocean through dissolved organic matter, *Nature*, 2005, **433**(7022), 142–145.
2 E. B. Kujawinski, The impact of microbial metabolism on marine dissolved organic matter, *Ann. Rev. Mar. Sci.*, 2011, **3**, 567–599.
3 L. Wang, Microbial control of the carbon cycle in the ocean, *Nat. Sci. Rev.*, 2018, **5**(2), 287–291.
4 T. S. Catala, S. Shorte and T. Dittmar, Marine dissolved organic matter: a vast and unexplored molecular space, *Appl. Microbiol. Biotechnol.*, 2021, **105**(19), 7225–7239.
5 O. J. Lechtenfeld, G. Kattner, R. Flerus, S. L. McCallister, P. Schmitt-Kopplin and B. P. Koch, Molecular transformation and degradation of refractory dissolved organic matter in the Atlantic and Southern Ocean, *Geochim. Cosmochim. Acta*, 2014, **126**, 321–337.
6 C. Patriarca, J. Bergquist, P. J. R. Sjoberg, L. Tranvik and J. A. Hawkes, Online HPLC-ESI-HRMS method for the analysis and comparison of different dissolved organic matter samples, *Environ. Sci. Technol.*, 2018, **52**(4), 2091–2099.
7 P. Li, J. Tao, J. Lin, C. He, Q. Shi, X. Li, *et al.*, Stratification of dissolved organic matter in the upper 2000 m water column at the Mariana Trench, *Sci. Total Environ.*, 2019, **668**, 1222–1231.
8 D. Petras, J. J. Minich, L. B. Cancelada, R. R. Torres, E. Kunselman, M. Wang, *et al.*, Non-targeted tandem mass spectrometry enables the visualization of organic matter chemotype shifts in coastal seawater, *Chemosphere*, 2021, **271**, 129450.
9 D. Petras, I. Koester, R. Da Silva, B. M. Stephens, A. F. Haas, C. E. Nelson, *et al.*, High-resolution liquid chromatography tandem mass spectrometry enables large scale molecular characterization of dissolved organic matter, *Front. Mar. Sci.*, 2017, **4**, 405.
10 L. Wegley Kelly, C. E. Nelson, D. Petras, I. Koester, Z. A. Quinlan, M. G. I. Arts, *et al.*, Distinguishing the molecular diversity, nutrient content, and energetic potential of exometabolomes produced by macroalgae and reef-building corals, *Proc. Natl. Acad. Sci. U. S. A.*, 2022, **119**(5), e2110283119.
11 Z. Zhou, Q.-L. Fu, M. Fujii and T. D. Waite, Complementary elucidation of the molecular characteristics of groundwater dissolved organic matter using ultrahigh-resolution mass spectrometry coupled with negative– and positive-Ion electrospray ionization, *Environ. Sci. Technol.*, 2023, **57**(11), 4690–4700.
12 L. Cancelada, R. R. Torres, J. Garrafa Luna, P. C. Dorrestein, L. I. Aluwihare, K. A. Prather, *et al.*, Assessment of styrene-divinylbenzene polymer (PPL) solid-phase extraction and non-targeted tandem mass spectrometry for the analysis of xenobiotics in seawater, *Limnol. Oceanogr.: Methods*, 2021, **20**(2), 89–101.
13 R. Antony, A. M. Grannas, A. S. Willoughbys, R. L. Sleighter, M. Thamban and P. G. Hatcher, Origin and sources of dissolved organic matter in snow on the East Antarctic ice sheet, *Environ. Sci. Technol.*, 2014, **48**(11), 6151–6159.
14 M. Gonsior, B. M. Peake, W. T. Cooper, D. C. Podgorski, J. D'Andrilli, T. Dittmar, *et al.*, Characterization of dissolved organic matter across the subtropical convergence off the South Island, New Zealand, *Mar. Chem.*, 2011, **123**(1–4), 99–110.
15 S. L. Felgate, A. J. Craig, L. W. K. Moodie and J. Hawkes, Characterization of a newly available coastal marine dissolved organic matter reference material (TRM-0522), *Anal. Chem.*, 2023, **95**(16), 6559–6567.
16 D. Bergmann, J. Matarrita-Rodriguez and H. Abdulla, Toward a more comprehensive approach for dissolved organic matter chemical characterization using an Orbitrap Fusion Tribrid mass spectrometer coupled with ion and liquid chromatography techniques, *Anal. Chem.*, 2024, **96**(9), 3744–3753.
17 Y. L. Qi, P. Q. Fu, S. L. Li, C. Ma, C. Q. Liu and D. A. Volmer, Assessment of molecular diversity of lignin products by various ionization techniques and high-resolution mass spectrometry, *Sci. Total Environ.*, 2020, **713**, 136573.
18 L. Xie, B. Wang, X. Pu, M. Xin, P. He, C. Li, *et al.*, Hydrochemical properties and chemocline of the Sansha Yongle Blue Hole in the South China Sea, *Sci. Total Environ.*, 2019, **649**, 1281–1292.
19 T. Li, A. Feng, Y. Liu, Z. Li, K. Guo, W. Jiang, *et al.*, Three-dimensional (3D) morphology of Sansha Yongle Blue Hole in the South China Sea revealed by underwater remotely operated vehicle, *Sci. Rep.*, 2018, **8**(1), 17122.
20 T. Dittmar, B. Koch, N. Hertkorn and G. Kattner, A simple and efficient method for the solid-phase extraction of dissolved organic matter (SPE-DOM) from seawater, *Limnol. Oceanogr.: Methods*, 2008, **6**, 230–235.
21 S. Heuckeroth, T. Damiani, A. Smirnov, O. Mokshyna, C. Brungs, A. Korf, *et al.*, Reproducible mass spectrometry data processing and compound annotation in MZmine 3, *Nat. Protoc.*, 2024, **19**(9), 2597–2641.
22 K. Duhrkop, M. Fleischauer, M. Ludwig, A. A. Aksenov, A. V. Melnik, M. Meusel, *et al.*, SIRIUS 4: a rapid tool for turning tandem mass spectra into metabolite structure information, *Nat. Methods*, 2019, **16**(4), 299–302.

23 M. Ludwig, L.-F. Nothias, K. Dührkop, I. Koester, M. Fleischauer, M. A. Hoffmann, *et al.*, Database-independent molecular formula annotation using Gibbs sampling through ZODIAC, *Nat. Mach. Intell.*, 2020, **2**(10), 629–641.
24 P. Li, W. Liang, Y. Zhou, Y. Yi, C. He, Q. Shi, *et al.*, Hypoxia diversifies molecular composition of dissolved organic matter and enhances preservation of terrestrial organic carbon in the Yangtze River Estuary, *Sci. Total Environ.*, 2024, **906**, 167661.
25 P. Kebarle and U. H. Verkerk, Electrospray: from ions in solution to ions in the gas phase, what we know now, *Mass Spectrom. Rev.*, 2009, **28**(6), 898–917.
26 U. Alcolombri, F. J. Peaudecerf, V. I. Fernandez, L. Behrendt, K. S. Lee and R. Stocker, Sinking enhances the degradation of organic particles by marine bacteria, *Nat. Geosci.*, 2021, **14**(10), 775.
27 C. Pelikan, K. Wasmund, C. Glombitza, B. Hausmann, C. W. Herbold, M. Flieder, *et al.*, Anaerobic bacterial degradation of protein and lipid macromolecules in subarctic marine sediment, *ISME J.*, 2021, **15**(3), 833–847.
28 Z. L. Chen, H. Zhang, Y. Yi, Y. He, P. Li, Y. Wang, *et al.*, Dissolved organic matter composition and characteristics during extreme flood events in the Yangtze River Estuary, *Sci. Total Environ.*, 2024, **914**, 169827.
29 N. B. Cech and C. G. Enke, Practical implications of some recent studies in electrospray ionization fundamentals, *Mass Spectrom. Rev.*, 2001, **20**(6), 362–387.
30 E. B. Kujawinski, K. Longnecker, N. V. Blough, R. D. Vecchio, L. Finlay, J. B. Kitner, *et al.*, Identification of possible source markers in marine dissolved organic matter using ultrahigh resolution mass spectrometry, *Geochim. Cosmochim. Acta*, 2009, **73**(15), 4384–4399.
31 M. Sun, W. Dai and D. Q. Liu, Fragmentation of aromatic sulfonamides in electrospray ionization mass spectrometry: elimination of SO_2 *via* rearrangement, *J. Mass Spectrom.*, 2008, **43**(3), 383–393.
32 A. Kruve and K. Kaupmees, Adduct formation in ESI/MS by mobile phase additives, *J. Am. Soc. Mass Spectrom.*, 2017, **28**(5), 887–894.
33 J. Beardall, M. Bjork and S. Beer, *Photosynthesis in the Marine Environment*, Wiley Blackwell, 2014, p. 224.
34 H. Ibrahim and L. Tremblay, Origin of dissolved organic sulfur in marine waters and the impact of abiotic sulfurization on its composition and fate, *Mar. Chem.*, 2023, **254**, 104273.
35 E. Magnuson, I. Altshuler, N. J. Freyria, R. J. Leveille and L. G. Whyte, Sulfur-cycling chemolithoautotrophic microbial community dominates a cold, anoxic, hypersaline Arctic spring, *Microbiome*, 2023, **11**(1), 203.
36 N. V. Patin, Z. A. Dietrich, A. Stancil, M. Quinan, J. S. Beckler, E. R. Hall, *et al.*, Gulf of Mexico blue hole harbors high levels of novel microbial lineages, *ISME J.*, 2021, **15**(8), 2206–2232.
37 H. A. Abdulla, D. J. Burdige and T. Komada, Abiotic formation of dissolved organic sulfur in anoxic sediments of Santa Barbara Basin, *Org. Geochem.*, 2020, **139**, 103879.
38 G. V. Gomez-Saez, T. Dittmar, M. Holtappels, A. M. Pohlabeln, A. Lichtschlag, B. Schnetger, *et al.*, Sulfurization of dissolved organic matter in the anoxic water column of the Black Sea, *Sci. Adv.*, 2021, **7**(25), eabf6199.
39 G. Y. Li and G. M. Huang, Alleviation of ion suppression effect in sonic spray ionization with induced alternating current voltage, *J. Mass Spectrom.*, 2014, **49**(7), 639–645.
40 H. Trufelli, P. Palma, G. Famiglini and A. Cappiello, An overview of matrix effects in liquid chromatography-mass spectrometry, *Mass Spectrom. Rev.*, 2011, **30**, 491–509.
41 S. Kim, L. A. Kaplan and P. G. Hatcher, Biodegradable dissolved organic matter in a temperate and a tropical stream determined from ultra-high resolution mass spectrometry, *Limnol. Oceanogr.*, 2006, **51**(2), 1054–1063.
42 M. Seidel, M. Beck, T. Riedel, H. Waska, I. G. N. A. Suryaputra, B. Schnetger, *et al.*, Biogeochemistry of dissolved organic matter in an anoxic intertidal creek bank, *Geochim. Cosmochim. Acta*, 2014, **140**, 418–434.
43 A. Reis, M. R. Domingues, P. Domingues, A. J. Ferrer-Correia and M. A. Coimbra, Positive and negative electrospray ionisation tandem mass spectrometry as a tool for structural characterisation of acid released oligosaccharides from olive pulp glucuronoxylans, *Carbohydr. Res.*, 2003, **338**(14), 1497–1505.
44 J. Hofmann, H. S. Hahm, P. H. Seeberger and K. Pagel, Identification of carbohydrate anomers using ion mobility-mass spectrometry, *Nature*, 2015, **526**(7572), 241–244.
45 S. Sun, Y. Liu, C. Weng, S. Sun, F. Li, H. Li, *et al.*, Cyclic dipeptides mediating quorum sensing and their biological effects in *Hypsizygus marmoreus*, *Biomolecules*, 2020, **10**(2), 298.
46 J. Pei, S. Chen, K. Yu, J. Liang, R. Zhang, P. Li, *et al.*, Microbial regulation of dissolved organic matter revealed by integrated metabolomics and metagenomics in the world's deepest blue hole, *Mar. Environ. Res.*, 2025, DOI: **10.1016/j.marenvres.2025.107354**.
47 J. I. Obeme-Nmom, R. O. Abioye, S. S. R. Flores and C. C. Udenigwe, Regulation of redox enzymes by nutraceuticals: a review of the roles of antioxidant polyphenols and peptides, *Food Funct.*, 2024, **15**(22), 10956–10980.
48 L. De Rossi, G. Rocchetti, L. Lucini and A. Rebecchi, Antimicrobial potential of polyphenols: mechanisms of action and microbial responses—a narrative review, *Antioxidants*, 2025, **14**(2), 200.
49 E. Bae, I. J. Yeo, B. Jeong, Y. Shin, K. H. Shin and S. Kim, Study of double bond equivalents and the numbers of carbon and oxygen atom distribution of dissolved organic matter with negative-mode FT-ICR MS, *Anal. Chem.*, 2011, **83**(11), 4193–4199.
50 A. Hu, L. Han, X. Lu, G. Zhang and J. Wang, Global patterns and drivers of dissolved organic matter across Earth systems: insights from H/C and O/C ratios, *Fundam. Res.*, 2024, DOI: **10.1016/j.fmre.2023.11.018**.
51 C. A. Carlson, S. Liu, B. M. Stephens and C. J. English, DOM production, removal, and transformation processes in

marine systems, in, *Biogeochemistry of Marine Dissolved Organic Matter*, Academic Press, 3rd edn, 2024, pp. 137–246.
52 B. Chen, K. F. Yu, L. Fu, Y. X. Wei, J. Y. Liang, Z. H. Liao, *et al.*, The diversity, community dynamics, and interactions of the microbiome in the world's deepest blue hole: insights into extreme environmental response patterns and tolerance of marine microorganisms, *Microbiol. Spectr.*, 2023, **11**(6), e0053123.
53 C. J. Rebouche and H. Seim, Carnitine metabolism and its regulation in microorganisms and mammals, *Annu. Rev. Nutr.*, 1998, **18**, 39–61.